S. Afr. J. Chem., 2025, 79, 27–33
https://journals.co.za/content/journal/chem/

Cytotoxic effects of Green Synthesised *Canavalia rosea*-derived ZnO nanoparticles

Ramakrishnan Vasanthi[1]*, Vadivel Balamurugan

[1]*PG and Research Department of Biotechnology, Sri Vinayaga College of Arts and Science, Ulundurpet, Kallakurichi district,Tamil Nadu, India (Affiliated to Thiruvalluvar University-Vellore)*

ABSTRACT

The investigation confirms the biosynthesis of zinc oxide nanoparticles and their antiproliferative capacity; this is the preeminent study to utilise *Canavalia rosea* leaf and stem extracts. Characterization techniques including Energy-dispersive X-ray spectroscopy, X-ray Diffraction, Fourier-transform Infrared Spectroscopy, UV-Vis Spectroscopy, Field-Emission Scanning Electron Microscopy, and Photoluminescence reveal the structural properties. By employing the DPPH assay, the antioxidant capacity of Le-ZnONPs and Se-ZnONPs at various concentrations (µg ml^{-1}), including 31.25, 62.5, 125, and 250, was assessed. According to FESEM analysis, the agglomerates of irregular-shaped zinc nanoparticles have a size range of 50 to 100 nm. In the DPPH assay, the antioxidant activity of both ZnONPs presented a more favourable response, with inhibition ranging from 80 to 90 percent. The cytotoxic effect of ZnONPs on MCF-7 cells was assessed by determining the IC_{50} values for Le-ZnONPs (52.08 µg ml^{-1}) and Se-ZnONPs (636.3 µg ml^{-1}). The substantial outcomes associated with the cytotoxic and antioxidant capacities of ZnONPs indicate that they may possess antiproliferative properties.

KEYWORDS

***in-vitro* cytotoxicity; zinc nanoparticles; *Canavalia rosea*; MCF-7; FE-SEM; FTIR analysis**

Received 6 December 2023, revised 28 January 2024, accepted 5 February 2025

INTRODUCTION

Current advancements are being made in the field of nanotechnology, which is an intersection of nanoscience and technology. It is concerned with the functions and properties of particular structures and elements of materials ranging in size from 1 to 100 nm. The software demonstrates functional applicability across various domains, such as engineering, material science, physics, chemistry, biology, computer science, biomedicine, diagnosis, drug delivery, and molecular imaging.[1,2] The present progress in the integration of nanomaterials with pharmaceutical products makes a substantial contribution to the detection of biomarkers, including nanobiochips, nanoelectrodes, nanobiosensors, and others.[3] In addition, nanomaterials offer improved resolutions for ecological and methodological challenges pertaining to water recycling, catalysis, and solar energy transfer.[4,5,6]

Nanomaterials are minuscule entities, with dimensions on the nanoscale, and they possess improved thermal conductivity and chemical stability due to their increased surface area-to-volume ratio.[7] Inorganic metal oxides, such as zinc oxide, copper oxide, and titanium oxide, are frequently employed in the fabrication of nanomaterials. Among these alternatives, ZnO-NPs are predominantly utilised due to their economical, secure, and uncomplicated synthesis processes.[8] Additionally, the USFDA[9] classifies ZnO as a GRAS [generally recognised as safe] metal oxide.

At present, the synthesis of nanoparticles via biological approaches is primarily conducted using actinomycetes, bacteria, fungi, yeast, and plant extracts. This approach circumvents the limitations associated with conventional methods.[10,11,12] For the ecological synthesis of nanoparticles using metal ions, plants are the predominant substrate source.[13,14] Various botanical components, including seeds, fruits, leaves, roots, stems, flowers, and fruits, are utilised in the synthesis of zinc oxide nanoparticles.[15,16,17,18] The biological approach offers several advantages, including cost-effectiveness, time efficiency, product stability, and ecological safety. Moreover, progenitor sources and intermediary agents are omitted.[19] Plant-derived phytoconstituents, including phenolic constituents, alkaloids, terpenoids, and flavonoids, distinguish them from alternative sources.[19,20] Antioxidants are substances that have the ability to counteract reactive oxygen species [ROS], free radicals, and metal chelation.[21] From this point forward, in order to produce metal oxide nanoparticles biochemically, antioxidants are the only stable and indispensable source, owing to their ability to reduce or chelate metals.[22,23]

Canavalia rosea, a plant found in coastal dunes, serves as the subject of this research concerning the environmentally friendly synthesis of zinc oxide nanoparticles. *Canavalia rosea's* aerial portions and roots are utilised in traditional medicine to treat a variety of ailments. Certain countries utilise the leaves as an alternative to smoking botanicals.[24] Mellow seeds that have been roasted are substituted for coffee in the West Indies. The seeds are ingested by both fauna and humans in West Africa as a source of protein.[25] Infusion of the root is applied topically to cure rheumatism, colds, skin disorders, and general pain.[26] On the whole, *Canavalia*[27] seeds contain between 31.2 and 35.5% protein and a minimal fat content. Additionally, the fibre content (1.1 and 10.2%) inhibits colon cancer and aids in the regulation of digestion, detoxification, and bowel movement, in addition to reducing blood cholesterol.[28]

This is the foremeost study to investigate the eco-friendly production of zinc oxide nanoparticles using extracts of *Canavalia rosea* leaves and stems. The main aim of this research is to assess and characterise the cytotoxic and antioxidant properties of zinc oxide nanoparticles (ZnONPs) in the MCF-7 cell line. This will provide valuable information regarding the antiproliferative potential of ZnO nanoparticles in the context of breast cancer.

MATERIALS AND METHODS

Collection and authentication of plants

Our experiment utilises the aerial components of *Canavalia rosea*, specifically the leaf and stem. Samiyarpettai, Cuddalore district, Tamil Nadu, India, possessed a plethora of coastal regions in the *C. rosea* vegetation. The herbarium specimen underwent identification and authentication by the Rapinet Herbarium, Department of Botany, St. Joseph Autonomous College, Tiruchirappalli, Tamil Nadu, India, to confirm its identity as *Canavalia rosea*.

*To whom correspondence should be addressed
Email: vasuramphd@gmail.com

ISSN 1996-840X Online / South African Chemical Institute / http://saci.co.za/journal

https://doi.org/10.17159/0379-4350/2025/v79a04

Materials

All the materials used in our study were purchased from Nice Chemicals and Sigma-Aldrich.

Preparation of leaf and stem extract

In an Erlenmeyer flask, approximately 10 grams (g) of the shade-dried crude powder of leaf and stem extract was infused with 100 millilitres (ml) of methanol. The concoction was heated for 20 minutes at 60°C in a heating mantle before being incubated at 37°C. Following a 24-hour incubation period, the supernatant was transferred into a sterile receptacle via filtration using Whatman filter paper No.1 (pore size = 11 micrometre (µm). The supernatant was stored in the refrigerator.

Green synthesis of zinc oxide nanoparticles

The extract and the 6 percentage (%) zinc nitrate salt were combined and stirred for 30 minutes at 60°C using a magnetic stirrer. After undergoing two washes with double-distilled water, the precipitate was transferred to a crucible and heated for four hours at 400°C in a muffle furnace. The precipitate was transferred to a crucible and heated for four hours at 400°C in a muffle furnace. For subsequent use, the powdered ZnONPs (white in colour) that have been dried in a sterile mortar were placed in sterile Eppendorf containers.

Nanoparticle characterisation

X-ray diffraction was employed to validate the crystalline structure of Le-ZnONPs and Se-ZnONPs. This was accomplished utilising a SHIMADZU-6000 Spectrofluorometer and monochromatic Cu-Kα radiation within the wavelength range of 1.5406˝. The XRD results are represented by peaks observed at different wavelengths spanning from 5 to 80 degrees at a 2θ angle. These peaks have been verified against ICDD (JCPDS) data. Utilising UV-visible spectroscopy analysis to validate the formation of zinc oxide nanoparticles is a crucial step. It contains UV and visible spectra. Spectral data spanning 0-1200 nm was monitored using a JASCO V-670 spectrophotometer. Prologue 3-HORIBAJOBINYVON assists in validating the photoluminescence spectrum [PL] within the wavelength range of 400 to 700 nm at ambient temperature. The documentation of the nanoparticles' structural properties is achieved via FESEM analysis conducted with a ZEISS-SIGMA microscope. By means of EDS analysis, the elemental components of Le-ZnONPs and Se-ZnONPs are identified. The two-dimensional spatial distribution of chemical element energy dispersion is validated via EDS mapping.

DPPH Assay

The DPPH assay is a practical and precise method for quantifying the activity of free radical scavenging. The methodology outlined in Blois method[29] is adhered to with only minor adjustments. A solution of DPPH (0.1 millimolar (mM)) is formulated by adding 1 ml of methanol-prepared DPPH to 3 ml of ZnO-NPs at five distinct concentrations (31.25, 61.25, 125 and 250 µg ml^{-1}). An absorbance of 517 nm was measured following a 10-minute incubation period. For calculating the percentage of radical scavenging values, the following formula is used:

$$\text{Percentage of inhibition} = [[A_o\text{-}A_1] / A_o] \times 100$$

where A_o represents the control's absorbance and A_1 represents the sample's absorbance.

In-vitro study

Cell culture maintenance

MCF-7 cells were obtained from the National Centre for Cell Science (NCCS), Pune, and were cultured in DMEM containing 10% fetal bovine serum (FBS), 1% glutamine, and 1% penicillin-streptomycin at 37°C in an incubator with 5% CO_2 and a humidified atmosphere. In the subculture, a monolayer of cells is utilised. Following a wash with phosphate-buffered saline [PBS] and trypsinization at 37°C for two to three minutes, the cells are transferred into new culture flasks that contain a medium. For each experiment, cells stocked between the third and fifth passages were utilised.

MTT Assay

The MTT assay is utilised to quantify the cytotoxic impact of Le-ZnONPs and Se-ZnONPs by observing the activity of mitochondrial dehydrogenase in living cells.[30] MCF-7 cells were cultured in a 96-well plate at a concentration of $1x10^6$ cells ml^{-1} and incubated at 37 °C for 24 hours. In specified wells, the cells were subjected to treatment with various concentrations of Le-ZnONPs and Se-ZnONPs [1.95, 3.9, 7.8, 15.6, 31.25, 62.5, 125, and 250 (µg ml^{-1})]. Each well was supplemented with 100 L of MTT solution [mg ml^{-1}] following a 72-hour incubation period at 37°C. The dishes are incubated at 37°C for four hours. Consequently, the formazan crystals were dissolved by adding 100 µl of DMSO to each well while the MTT medium was aspirated from each well without disturbing the cells. At 570 nanometers, the absorbance was measured using a microplate reader [Tecan Multimode Multiwall Plate Reader, Austria]. The assays were conducted in triplicate, each independently.

The calculation for percentage cell viability is as follows:

$$\text{Percentage of Cell Viability} = \frac{\text{Optical density of the sample}}{\text{Optical density of control}} \times 100$$

RESULTS AND DISCUSSION

The objective of this research is to ascertain the physical and structural characteristics of ZnONPs, as well as their antioxidant capacity, ability to scavenge reactive oxygen species (ROS), and apoptotic effect. In order to produce zinc nanoparticles, zinc nitrate is utilised as a precursor. Both extracts are utilised in the synthesis of nanoparticles as thickening or capping agents. The colour change indicates the formation of ZnONPs; the Le-ZnONPs appeared pastel yellow, while the Se-ZnONPs were off-white in hue.

Diverse nanoparticle shapes and sizes are influenced by physical parameters including calcination temperature, precursor used, temperature during nanoparticle synthesis, pH, and the presence of stabilising agents. The precursor substances employed in the synthesis of nanoparticles influence both the dimensions and morphology of the nanomaterials. The zinc chloride, nitrate, and zinc sulphate nanoparticles have the morphology of flakes.[31] The synthesis and calcination temperatures for zinc nanoparticles were approximately 60°C for 30 minutes and 400°C for 4 hours, respectively. Using zinc nitrate as a precursor, spherical flake-shaped agglomerates of ZnO nanoparticles ranging in size from 50 to 200 nm are synthesised at a neutral pH. Furthermore, some reports suggest that the NPs transform into flake-shaped aggregates when zinc nitrate is used as a precursor.[32]

X-ray diffraction

Figure 1 demonstrates intensity plotted against 2θ. The findings suggest that the Le-ZnONPs possess the structure of crystalline hexagonal wurtzite. Seven relatively high diffraction peaks emanating from the [1 0 0], [0 0 2], [1 0 1], [1 0 2], [1 1 0], [1 0 3], and [112] reflections of the hexagonal ZnO crystal were observed in the XRD patterns of both Le-ZnONPs and Se-ZnONPs. The peaks that are displayed in the data have been indexed using ICDD (JCPDS) data [card number 36-1451]. The absence of additional impurity peaks in this region suggests that the products formed during the nanoparticles' formation are relatively pure.

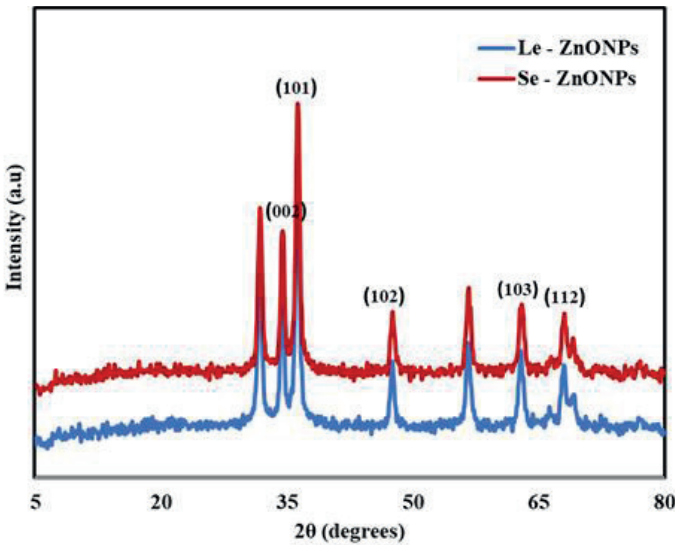

Figure 1. The XRD diffraction spectrum of Le-ZnONPs and Se-ZnONPs.

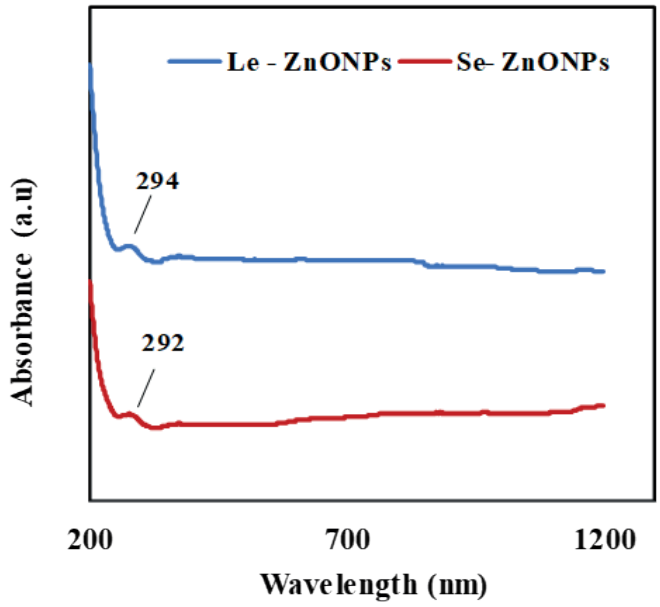

Figure 2. Spectrum of UV-visible spectroscopic absorption by Le-ZnONPs and Se-ZnONPs.

By confirming the phase of synthesised zinc oxide nanoparticles, X-ray diffraction is utilised. The distinct peaks observed in Figure 1 underscore the crystalline characteristics of Le-ZnONPs and Se-ZnONPs. The Miller indices values validate that the ZnO nanoparticles that were produced exhibit face-centered cubic symmetry. Previous studies have examined the Miller indices values [100], [002], [101], [102], [110], [103], and [112] obtained from zinc oxide nanoparticles produced with *Parthenium hysterophorus L.* leaf extract, which provides further evidence for the crystalline nature of the nanoparticles.[33] The Miller indices values obtained for the zinc nanoparticles synthesised from both the leaf and stem extracts were consistent with those reported in prior research that examined the crystallinity of zinc oxide nanoparticles.[34,35]

Ultraviolet-visible spectroscopy

The UV spectroscopic analysis of Le-ZnONPs and Se-ZnONPs and their absorbance patterns are depicted in Figure 2. At approximately 300 nanometers, the spectrum analysis reveals the formation of nanoparticles via an absorbance peak. Le-ZnONPs exhibited a clear peak at 294 nanometers. In a similar fashion, the Se-ZnONPs exhibited a peak at 292 nm that varied minimally. The formation of the absorbance peak occurs as a result of an electron transition from the valence band to the conduction band subsequent to the absorption of light. When the excitation of surface plasmon resonance detects a colour transition from green to yellowish-white in a suspension, UV-Visible spectroscopy verifies the formation of ZnONPs.

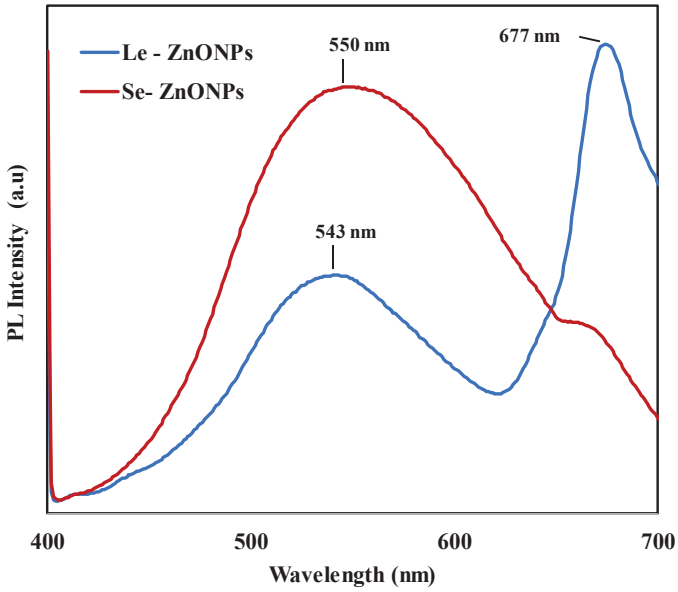

Figure 3. Photoluminescence spectrum Le-ZnONPs and Se-ZnONPs.

Photoluminescence

Photoluminescence serves as a highly efficient method for ascertaining the optical characteristics of nanoparticles. The emission spectrum is observed at 400 nanometers excitation wavelength at ambient temperature. The PL spectrum of Le-ZnONPs and Se-ZnONPs is illustrated in Figure 3. Two peaks were identified in the Le-ZnONPs sample, an initial peak at 542 nm, corresponds to green emission and a subsequent peak at 677 nm corresponds to red emission spectrum. Similarly, two peaks were noted for Se-ZnONPs. The peaks observed at 550 and 570 nm of Se-ZnONPs correspond to green emission. The emission peaks observed in the ultraviolet and visible regions may be attributed to defect states and bound excitons located on the surface of nanostructured ZnONPs.[36,37]

FESEM and EDAX analysis

Through FE-SEM analysis, the dimensions and morphology of the manufactured ZnONPs are classified. Figure 4a and Figure 4b illustrate the FESEM electron micrographs of Se-ZnONPs and Le-ZnONPs, respectively. The morphology of ZnONPs is irregularly shaped. FE-SEM images further demonstrate that the dimensions of both ZnO nanoparticles span a range of 50 to 200 nm. The elemental composition and EDAX chromatogram pattern of Le-ZnONPs are illustrated in Figure 4c. The weight percentage of each ion, specifically oxygen and zinc atoms, is disclosed in this study. The elemental composition of Zn and O in the Se-ZnONPs is verified in Figure 4d. In a hypothetical scenario, Le-ZnONPs exhibited the likely stoichiometric mass percentages of Zn and O to be approximately 32.8% and 67.2%, respectively. In contrast, Se-ZnONPs revealed these mass percentages as 69.14% and 30.86%, respectively. The surface analysis of Le–ZnONPs and Se–ZnONPs using field emission scanning electron microscopy (FESEM) is illustrated in Figure 4a and 4b, respectively. The dimensions and configuration of the ZnONPs are disclosed by FE-SEM, while their elemental composition is determined by EDS methods. The presence of oxygen and zinc ions in the synthesised ZnONP was identified by EDS analysis, thereby validating the nanoparticles' purity.

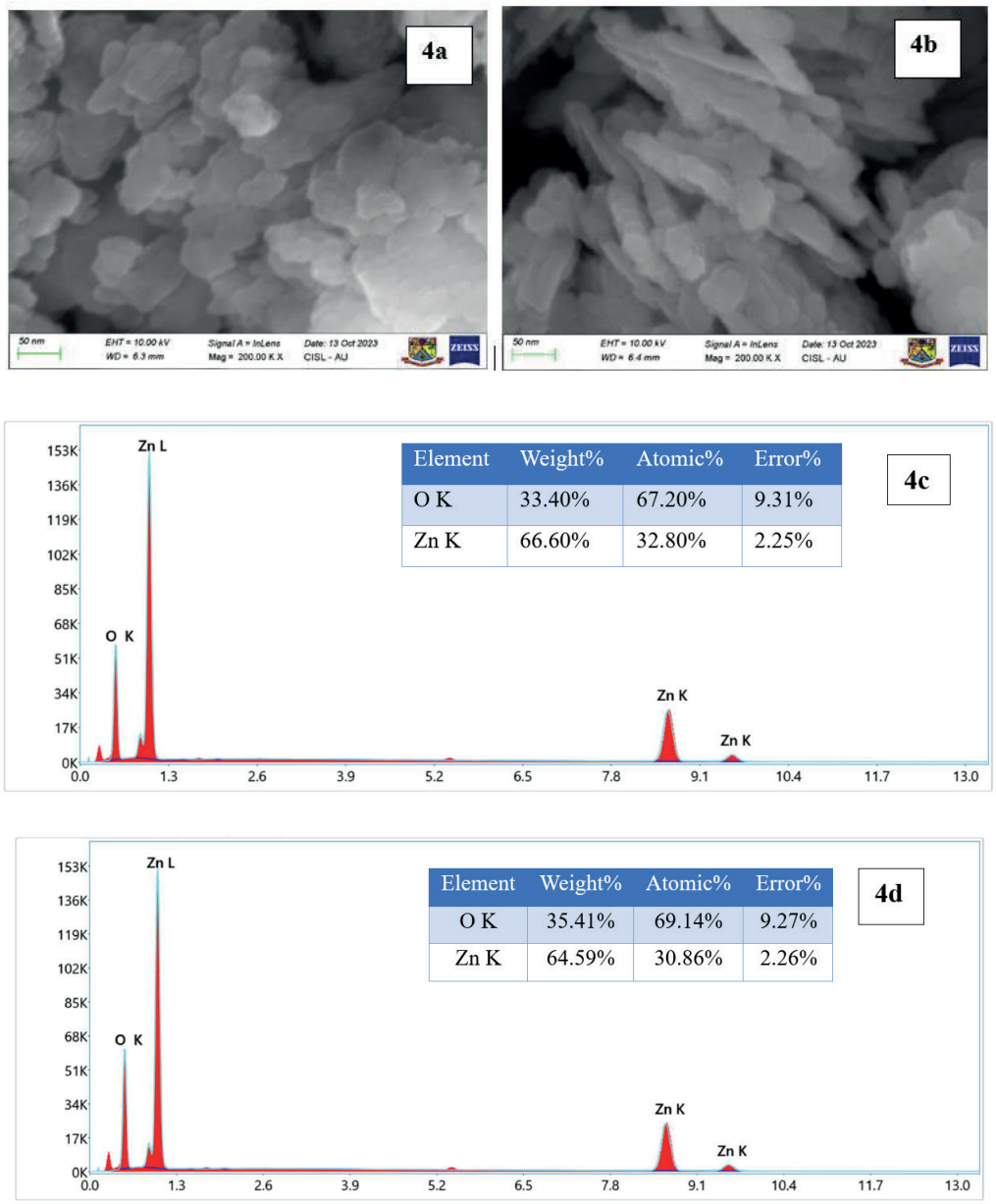

Figure 4: (a and b) FESEM analysis of Le-ZnONPs and Se–ZnONPs. (c) Le–ZnONP's elemental composition and EDX chromatogram. (d) Elemental composition and EDX chromatogram of Se-ZnONPs.

Fourier Transform Infrared Spectroscopy

FTIR is a highly effective method for identifying chemical components due to the fact that each molecule[38] has a distinct molecular pattern. Firm-adherent functional groups on the surface of nanoparticles can be verified using FTIR[39]. Figure 5 denotes the FTIR constituents of natural stem and leaf extract, in addition to Le-ZnONPs and Se-ZnONPs. The peak patterns of the unrefined leaf and stem extract were comparable, with minor variations. The FTIR analysis of the natural leaf extract reveals distinct bands at the following wavenumbers: 3446.02 cm^{-1}, 2918.49 cm^{-1}, 2850.14 cm^{-1}, 1647.00 cm^{-1}, 1384.51 cm^{-1}, 1068.82 cm^{-1}, 606.85 cm^{-1}, and 423.71 cm^{-1}. The peaks observed at 2918.49 cm^{-1} and 3446.02 cm^{-1}, respectively, are indicative of the stretching of hydroxyl compounds and the C-H bond. The peaks observed at a wavenumber of 1384.51 cm^{-1} and 1647.00 cm^{-1} are corresponding to aromatic nitro compounds and secondary alcohol, respectively. The peak at 1068.82 cm^{-1} is indicative of the C-N or C-O bond of the primary amine or alcohol, respectively. The peak observed at 423.71 cm^{-1} is indicative of the metal-oxygen (Zn-O) bond.

In a similar fashion, the banding patterns observed at 3420.91 cm^{-1}, 2919.24 cm^{-1}, 1731.20 cm^{-1}, 1635.39 cm^{-1}, 1423.61 cm^{-1}, 1260.72 cm^{-1}, 1053.52 cm^{-1}, and 592.17 cm^{-1} are confirmed by the pure stem extract. Similarly, the formation of peaks at 3424.64 cm^{-1}, 2921.04 cm^{-1}, 1631.52 cm^{-1}, 1384.31 cm^{-1}, 878.37 cm^{-1}, and 423.71 cm^{-1} is confirmed by Le-ZnONPs. While the peaks observed for Se-ZnONPs are comparable to those for Le-ZnONPs, there are minor distinctions 3423.58 cm^{-1}, 1632.29 cm^{-1}, 1384.34 cm^{-1}, 893.42 cm^{-1}, and 435.52 cm^{-1} with the peaks. FTIR analysis identified the prominent bands that corresponded to particular functional groups. Alcoholic groups, primary or secondary amine groups, carboxylic acid groups, aldehyde and thiol groups, aromatic and anhydride groups are all viable functional groups.

DPPH Antioxidant Assay

The DPPH results of Le-ZnONPs and Se-ZnONPs are illustrated in Figure 6. The antioxidant capacity of leaf and stem extracts was assessed using ZnO-NPs at concentrations of 31.25, 62.5, 125, and 250 µg/ml. Several research studies[40,41,42] adhered to the identical methodology. As a reference standard, concentrations of gallic acid at which DPPH inhibition was measured were 82%, 78%, 72%, and 69% at 31.25, 62.5, 125, and 250 µg ml^{-1}, respectively. Le-ZnONPs exhibited inhibition

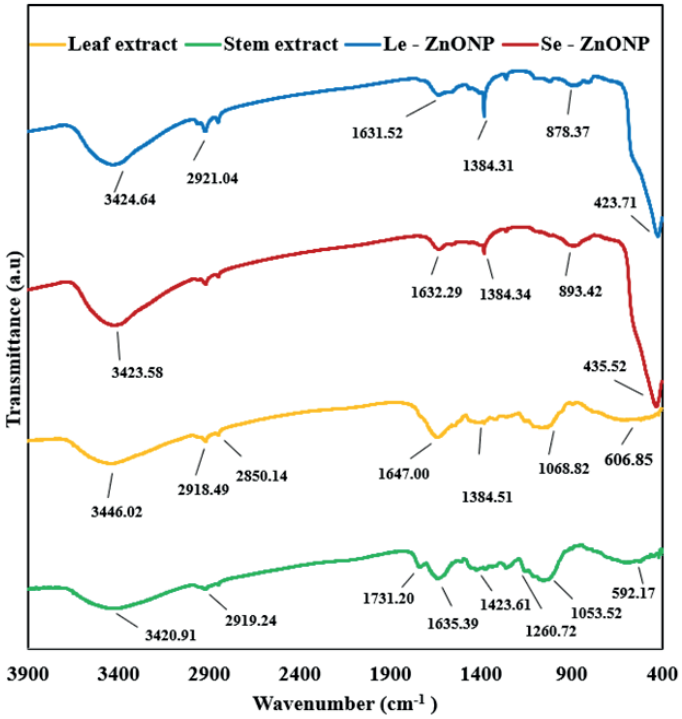

Figure 5. FTIR analysis of Le-ZnONPs and Se-ZnONPs.

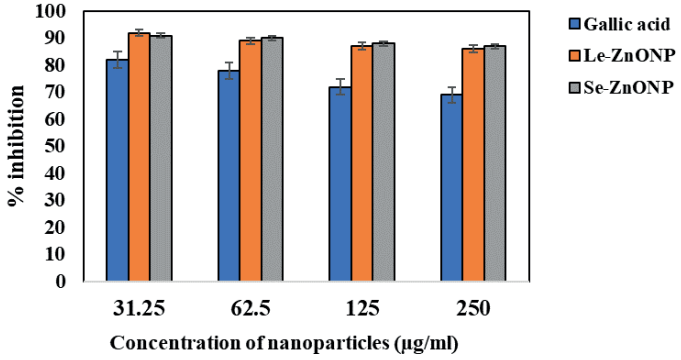

Figure 6. DPPH evaluation of ZnONPs. The values represent the mean (±SD) of three replicates.

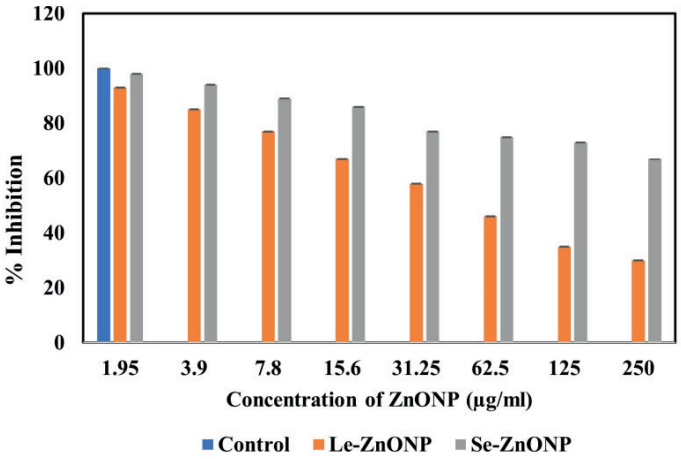

Figure 7. Evaluation of the cytotoxicity of Le-ZnONPs and Se-ZnONPs. The values represent the mean (±SD) of three replicates.

rates of 92%, 89%, 87%, and 86% at the respective test concentrations. The inhibition levels of Se-ZnONPs were correspondingly 91%, 90%, 88%, and 87%. The range of inhibition percentages for DPPH scavenging is nearly identical for Le-ZnONPs and Se-ZnONPs. The results of a statistical analysis using the T-test indicated a significant difference ($P < 0.05$) between gallic acid and zinc nanoparticles, as indicated by the P value of 0.005.

The percentage of free radical inhibition exhibited by both Le-ZnONPs and Se-ZnONPs indicates that the redox potential of phytochemicals present in the respective extracts is a substantial factor in the elimination of free radical molecules[43]. Therefore, it is generally accepted that the increased antioxidant activity could be attributed to the antioxidants' preferential adsorption onto the nanoparticle surface. The electron contribution of oxygen atoms is associated with the antioxidant activity of ZnO-NPs.[44] The free radicals DPPH are influenced by the plant extract's polyphenols and tocopherols via electron transfer or the donation of hydrogen atoms.[45]

In-vitro Cytotoxicity

The MTT assay is a preliminary method for determining the half-minimal inhibitory concentration [IC_{50}] and assessing proliferative activity. The impact of ZnO-NPs on the mitochondrial activity of MCF-7 cell lines is clarified in this study. By generating aerobic ATP, mitochondria are essential for maintaining cellular function; therefore, they are utilised to determine cytotoxicity.[46,47] The cytotoxic effect of nanoparticles is influenced by variables such as dosage and duration.

The assay was conducted using test concentrations of 1.95, 3.9, 7.8, 15.6, 31.25, 62.5, 125, and 250 (µg ml^{-1}) for both leaf and stem extracts. The percentage of viable cells for Le-ZnONPs was determined to be 93%, 85%, 77%, 67%, 58%, 46%, 35%, and 30%; for Se-ZnONPs, the percentage was 98%, 94%, 89%, 86%, 77%, 75%, 67%, 73%, and 67%, respectively. The results of an independent t-test indicate that Le-ZnONPs and Se-ZnONPs differ significantly, with a P value of 0.036, which is lower than the significance level of P=0.05. Le-ZnONPs and Se-ZnONPs each had IC_{50} values of 52.08 µg ml^{-1} and 636.3 µg ml^{-1}, respectively. The IC_{50} concentration was calculated using sigmoidal curve calculation in Microsoft Office Professional Plus 2021-Excel software.

The *in-vitro* cytotoxicity analysis provides further evidence that the ZnONPs exhibited substantial anticancer capabilities when tested on the MCF-7 cell line. The potential of the nanoparticles to breach the cell membrane and inhibit the mRNA expression of genes that promote the upregulation of reactive oxygen species (ROS) within the cell[48] is linked to cell demise. When ROS concentrations are so high, ZnONPs induce a deleterious response in the macromolecules and nucleus of the cell.[49] Membrane impairment may occur as a consequence of elevated ROS levels; this can be achieved via lipid peroxidation and protein denaturation, which in turn induce necrotic damage and apoptosis.[50] Apoptosis, which is characterised by diminished cell size, a condensed nucleus, membrane damage, and disintegrated apoptotic groups bonded to the membrane, is characterised by structural attributes of programmed cell death. These attributes culminate in phagocytosis.[51] Several reports have documented comparable findings.[50,52,53] The in vitro investigations validated that both Le-ZnONPs and Se-ZnONPs induce a substantial decrease in cell viability when applied to the MCF-7 cell line.

CONCLUSION

The study verifies the viability of producing ZnO nanoparticles via biogenic synthesis using extracts of the leaves and stems of *Canavalia rosea*. The antiproliferative activity of the leaf and stem extracts is ascribed to the phytochemical components that are found within the extracts. Zinc nanoparticles demonstrate noteworthy outcomes in vitro; additional investigation into this field may yield a more effective material for biomedical applications. As the first study to report ZnONP synthesis and cytotoxicity analysis using *Canavalia rosea*, suitable in-vivo experiments could enrich the nanomaterials for therapeutic applications.

AUTHOR CONTRIBUTIONS

Ramakrishnan Vasanthi: Investigation, data curation, methodology, formal analysis, writing-original draft preparation and editing.
Balamurugan Vadivel: Conceptualization, supervision, validation, writing-review and editing.

ACKNOWLEDGEMENTS

The authors are grateful to the Management, Department of Biotechnology, Physics, and Chemistry, of Sri Vinayaga College of Arts and Science, Ulundurpet, Tamilnadu, India for providing laboratory facilities. We are thankful to the Department of Nanoscience, Karunya Institute of Technology and Sciences, Coimbatore, and Centralised Instrumentation and Service Laboratory, Department of Physics, Annamalai University, Tamilnadu, India for providing facilities for the part of the research work.

ORCID IDS

Ramakrishnan Vasanthi: https://orcid.org/0000-0002-9557-1169
Vadivel Balamurugan: https://orcid.org/0000-0001-7234-4206

REFERENCES

1. Bayda S, Adeel M, Tuccinardi T, Cordani M, Rizzolio F. The History of Nanoscience and Nanotechnology: From Chemical–Physical Applications to Nanomedicine. Molecules. 2020;*25*:112. https://doi.org/10.3390/molecules25010112.
2. Kinnear C, Moore TL, Rodriguez-Lorenzo L, Rothen-Rutishauser B, Petri-Fink A. Form Follows Function: Nanoparticle Shape and Its Implications for Nanomedicine. Chem Rev. 2017;117:11476–11521. https://doi.org/10.1021/acs.chemrev.7b00194
3. Weissig V, Pettinger TK, Murdock. Nanopharmaceuticals (part 1): Products on the market. Int J Nanomed. 2014; 9:4357–4373. https://doi.org/ 10.2147/IJN.S46900.
4. Ismael M. A review and recent advances in solar-to-hydrogen energy conversion based on photocatalytic water splitting over doped-TiO2 nanoparticles. Sol Energy. 2020;211:522–546. https://doi.org/10.1016/j.solener.2020.09.073.
5. Saied E, Eid AM, Hassan SED, Salem SS, Radwan AA, Halawa M, Saleh FM, Saad HA, Saied EM, Fouda A. The Catalytic Activity of Biosynthesized Magnesium Oxide Nanoparticles (MgO-NPs) for Inhibiting the Growth of Pathogenic Microbes, Tanning Effluent Treatment, and Chromium Ion Removal. *Catalysts.* 2021;*11*:821. https://doi.org/10.3390/catal11070821.
6. Saied E, Salem SS, Al-Askar AA, Elkady FM, Arishi AA, Hashem AH. Mycosynthesis of Hematite (α-Fe^2O^3) Nanoparticles Using *Aspergillus niger* and Their Antimicrobial and Photocatalytic Activities. Bioengineering. 2022;9:397. https://doi.org/10.3390/bioengineering9080397.
7. Agarwal H, Kumar SV, Rajeshkumar S. A review on green synthesis of zinc oxide nanoparticles–an eco-friendly approach. Resource-Efficient Technologies. 2017;3(4):406–413. https://doi.org/10.1016/j.reffit.2017.03.002.
8. Jayaseelan C, Abdul Rahman A, Vishnu Kirthi A, Marimuthu S, Santhoshkumar T, Bagavan A, Gaurav K, Karthik L, Bhaskara Rao KV. Novel microbial route to synthesize ZnO nanoparticles using Aeromonas hydrophila and their activity against pathogenic bacteria and fungi. Spectrochim Acta A Mol Biomol Spectrosc. 2012;90:78–84. https://doi.org/10.1016/j.saa.2012.01.006.
9. Pulit-prociak J, Chwastowski A, Kucharski M, Banach M. Functionalization of textiles with silver and zinc oxide nanoparticles. Appl Surf Sci. 2016;385:543–553. https://doi.org/10.1016/j.apsusc.2016.05.167.
10. Syed B, Nagendra-Prasad MN, Satish S. Endogenic mediated synthesis of gold nanoparticles bearing bactericidal activity. J Microsc Ultrastruct. 2016;4(3):162–166. http://dx.doi.org/10.1016/j.jmau.2016.01.004.
11. Salem SS, Fouda A. Green synthesis of metallic nanoparticles and their prospective biotechnological applications: an overview. Biol Trace Elem Res. 2021;199(1):344–370. https://doi.org/10.1007/s12011-020-02138-3.
12. Salem S, Hammad EN, Mohamed AA, El-Dougdoug W. A comprehensive review of nanomaterials: types, synthesis, characterization, and applications. Biointerface Res Appl Chem. 2023;13(1):41. https://doi.org/10.33263/BRIAC131.041.
13. Iravani, S. Green synthesis of metal nanoparticles using plants. Green Chem. 2011;13:2638–2650. https://doi.org/10.1039c1gc15386b.
14. Kharissova OV, Rasika HV, Kharisov DBI, Perez BO, Jimenez Perez VM. The Greener Synthesis of Nanoparticles. Trends Biotechnol. 2013; 31:240–248. http//dx.doi.org/10.1016/j.tibtech.2013.01.003.
15. Altuwirqi RM, Albakri AS, Al-Jawhari H, Ganash EA. Green synthesis of copper oxide nanoparticles by pulsed laser ablation in spinach leaves extract. Optik 2020; 219:165280. http://dx.doi.org/10.1016/j.ijleo.2020.165280.
16. Asmat-Campos D, Abreu AC, Romero-Cano MS, Urquiaga-Zavaleta J, Contreras-Caceres R, Delfin-Narciso D, Juarez-Cortijo L, Nazario-Naveda R, Rengifo-Penadillos R, Fernandez I. Unraveling the Active Biomolecules Responsible for the Sustainable Synthesis of Nanoscale Silver Particles through Nuclear Magnetic Resonance Metabolomics. ACS Sustain. Chem. Eng. 2020;8:17816–17827. http://dx.doi.org/10.1021/acssuschemeng.0c06903.
17. Mohamed EA. Green synthesis of copper & copper oxide nanoparticles using the extract of seedless dates. Heliyon. 2020;6:e03123. https://doi.org/10.1016/j.heliyon.2019.e03123.
18. Siddiqui VU, Ansari A, Chauhan R, Siddiqi WA. Green synthesis of copper oxide (CuO) nanoparticles by *Punica granatum* peel extract. Mater. Today Proc. 2021;36:751–755. http://dx.doi.org/10.1016/j.matpr.2020.05.504.
19. Heinlaan M, Ivask A, Blinova I, Dubourguier HC, Kahru A. Toxicity of nano-sized and bulk ZnO, CuO and TiO2 to bacteria *Vibrio fischeri* and crustaceans *Daphnia magna* and *Thamnocephalus platyurus*. Chemosphere. 2008;71:1308–1316. https://doi.org/10.1016/j.chemosphere.2007.11.047.
20. Qu J, Yuan X, Wang X, Shao P. Zinc accumulation and synthesis of ZnO nanoparticles using *Physalis alkekengi* L, Environ Pollut. 2011;159:1783–1788. https://doi.org/10.1016/j.envpol.2011.04.016.
21. Flora SJS. Structural, chemical and biological aspects of antioxidants for strategies against metal and metalloid exposure. Oxid Med Cell Longev. 2009;2:191–206. https://doi.org/10.4161/oxim.2.4.9112.
22. Ahmed S, Ali S, Ikram S. A review on biogenic synthesis of ZnO nanoparticles using plant extracts and microbes: a prospect towards green chemistry. J Photochem Photobiol B Biol. 2017;166:272–284. https://doi.org/10.1016/jphotobiol.2016.12.011.
23. Anjum NA, Hasanuzzaman M, Hossain MA, Thangavel P, Roychoudhury A, Gill SS, Rodrigo MAM, Adam V, Fujita M, Kizek R, Duarte AC, Pereira E, Ahmad I. Jacks of metal/metalloid chelation trade in plants - An Overview. Front Plant Sci. 2015;6:1–17. https://doi.org/10.3389/fpls.2015.00192.
24. Seena S, Sridhar KR, Ramesh SR. Nutritional and protein quality evaluation of thermally treated seeds of Canavalia maritima in the rat. Nutr Res. 2005;25:587–596. https://doi.org/10.1016/j.nutres.2005.06.002.
25. Abbey BW, Ibeh GO. Functional properties of raw and heat processed brown bean [*Canavalia rosea* DC.] flour. J Food Sci. 1987;52:406–408. http://dx.doi.org/10.1111/j.1365-2621.1987.tb06625.x.
26. Seena S, Sridhar KR, Bhagya B. Biochemical and biological evaluation of an unconventional legume, *Canavalia maritima* of coastal dunes of India. Trop Subtrop Agroecosystems. 2005;5:1–14.
27. Arun AB, Sridhar KR, Raviraja NS, Schmidt E, Jung K. Nutritional and antinutritional components of Canavalia spp. seeds from the west coast sand dunes of India. Plant Foods Hum Nutr. 2003;58:1–13. https://doi.org/10.1023/B:QUAL.0000040340.86158.61.
28. Seena S, Sridhar KR. Nutritional and microbiological features of little-known legumes, *Canavalia cathartica Thouars* and *Canavalia maritima Thouars* of the southwest coast of India. Current Science.2006;90:1638–1650.
29. Blois M. Antioxidant Determinations by the Use of a Stable Free Radical. Nature. 1958;181:1199–1200. https://doi.org/10.1038/1811199a0.
30. Mosmann T. Rapid colorimetric assay for cellular growth and survival: application to proliferation and cytotoxicity assay. J Immunol Methods. 1983;65:55–63. https://doi.org/10.1016/0022-1759(83)90303-4.
31. Manabeng M, Mwankemwa BS, Ocaya RO, Motaung TE, Malevu TD. A Review of the Impact of Zinc Oxide Nanostructure Morphology on Perovskite Solar Cell Performance. Processes. 2022;10:1803. https://doi.org/10.3390/pr10091803.
32. Manikandan B, Endo T, Kaneko, S, Murali KR, John R. Properties of sol gel synthesized ZnO nanoparticles. Journal of Materials Science: Materials in Electronics. 2018;29:9474–9485. https://doi.org/10.1007/s10854-018-8981-8.

33. Rajiv P, Rajeshwari S, Venckatesh R. Bio-Fabrication of zinc oxide nanoparticles using leaf extract of *Parthenium hysterophorus* L. and its size-dependent antifungal activity against plant fungal pathogens. Spectrochim Acta A Mol Biomol Spectrosc. 2013; 112:384–387. https://doi.org/10.1016/j.saa.2013.04.072.
34. Jayarambabu N, Siva Kumari B, Venkateswara Rao K, Prabhu YT. Beneficial role of zinc oxide nanoparticles on green crop production. Int J Multidiscip Adv Res Trends.2015;2:273–282. https://doi.org/10.1007/s12210-015-0417-2.
35. Devi RS, Gayathri R. Green synthesis of zinc oxide nanoparticles by using *Hibiscus rosa-sinensis*. Int J Curr Eng Technol. 2014;4(4):2444–2446. http://inpressco.com/category/ijcet.
36. Nagaraju G, Prashanth SA, Shastri M, Yathish KV, Anupama C, Rangappa D. Electrochemical heavy metal detection, photocatalytic, photoluminescence, biodiesel production and antibacterial activities of Ag–ZnO nanomaterial. Mater Res Bull. 2017;94:54–63. https://doi.org/10.1016/j.materresbull.2017.05.043.
37. Basavalingiah KR, Harishkumar S, Udayabhanu, Nagaraju Dinesh Rangappa G, Chikkahanumantharayappa. Highly porous, honeycomb-like Ag–ZnO nanomaterials for enhanced photocatalytic and photoluminescence studies: green synthesis using *Azadirachta indica* gum. SN Applied Sciences. 2019;1:935 https://doi.org/10.1007/s42452-019-0863-z.
38. Taha M, Hassan M, Essa S, Tartor Y. Use of Fourier transform infrared spectroscopy [FTIR] spectroscopy for rapid and accurate identification of yeasts isolated from human and animals. Int J Vet Sci Med. 2013;1(1):15–20. https://doi.org/10.1016/j.ijvsm.2013.03.001.
39. Wolkers W, Oldenhof H. In situ FTIR assessment of dried *Lactobacillus bulgaricus*: KBr disk formation affects physical properties. Spectroscopy.2005;15:89–99. https://doi.org/10.1155/2005/216509.
40. Ochieng Nyalo P, Isanda Omwenga G, Piero Ngugi M. GC-MS Analysis, Antibacterial and Antioxidant Potential of Ethyl Acetate Leaf Extract of Senna singueana (Delile) Grown in Kenya. Evid Based Complement Alternat Med. 2022:5436476. https://doi.org/10.1155/2022/5436476.
41. Chiu HI, Che Mood CNA, Mohamad Zain NM, Ramachandran MR, Yahaya N, Nik Mohamed Kamal NNS, Tung WH, Yong YK, Lee CK, Lim V. Biogenic Silver Nanoparticles of *Clinacanthus nutans* as Antioxidant with Antimicrobial and Cytotoxic Effects. Bioinorg Chem Appl. 2021:9920890. https://doi.org/10.1155/2021/9920890.
42. Aliyu AB, Ibrahim MA, Ibrahim H, Musa AM, Lawal AY, Oshanimi JA, Usman M, Abdulkadir IE, Oyewale AO, Amupitan JO. Free radical scavenging and total antioxidant capacity of methanol extract of *Ethulia conyzoides* growing in Nigeria. Rom Biotechnol Lett. 2012;17(4):7458–7465.
43. Zheng W, Wang SY. Antioxidant activity and phenolic compounds in selected herbs. J Agric Food Chem. 2001;49:5165–5170. https://doi.org/10.1021/jf010697n.
44. Das D, Nath BC, Phukon P, Kalita A, Dolui SK. Synthesis of ZnO nanoparticles and evaluation of antioxidant and cytotoxic activity. Colloids Surf B: Biointerfaces. 2013;111:556–560. https://10.1016/j.colsurfb.2013.06.041.
45. Banerjee A, Dasgupta N, De B. *In vitro* study of antioxidant activity of Syzygium cumini fruit. Food Chem. 2005;90:727–733. https://doi.org/10.1016/j.foodchem.2004.04.033.
46. Meyer JN, Leung MC, Rooney JP, Sendoel A, Hengartner MO, Kisby GE, Bess AS. Mitochondria as a target of environmental toxicants. Toxicol Sci. 2013;134(1):1–17. https://doi.org/10.1093/toxsci/kft102.
47. Wallace KB, Starkov AA. Mitochondrial targets of drug toxicity. Ann Rev Pharmacol Toxicol. 2000;40:353–388. https://doi:10.1146/annurev.pharmtox.40.1.353.
48. Ma DD, Yang WX. Engineered nanoparticles induce cell apoptosis: potential for cancer therapy. Oncotarget. 2016;7:40882–40903. https://doi.org/10.18632/oncotarget.8553.
49. Vidovic S, Elder J, Medihala P, Lawrence JR, Predicala B, Zhang H, Korber DR. ZnO nanoparticles impose a panmetabolic toxic effect along with strong necrosis, inducing activation of the envelope stress response in *Salmonella enterica* serovar Enteritidis. Antimicrob Agents Chemother. 2015;59:3317–3328. https://doi.org/10.1128/AAC.00363-15.
50. Nita M, Grzybowski A. The Role of the Reactive Oxygen Species and Oxidative Stress in the Pathomechanism of the Age-Related Ocular Diseases and Other Pathologies of the Anterior and Posterior Eye Segments in Adults. Oxid Med Cell Longev. 2016:3164734. https://doi.org/10.1155/2016/3164734.
51. Saikumar P, Dong Z, Mikhailov V, Denton M, Weinberg JM, Venkatachalam MA. Apoptosis: definition, mechanisms, and relevance to disease. Am J Med. 1999;107(5):489–506. https://doi.org/10.1016/S0002-343[99]00259-4.
52. Schwartz GK, Shah MA. Targeting the cell cycle: a new approach to cancer therapy. J Clin Oncol. 2005;23:9408–9421. https://doi.org/10.1200/JCO.2005.01.5594.
53. Namvar F, Rahman HS, Mohamad R. Cytotoxic effect of magnetic iron oxide nanoparticles synthesized via seaweed aqueous extract. Int J Nanomed. 2014;9(1):2479–2488. https://doi.org/10.2147/IJN.S59661.